Naval Surface Warfare Center
Carderock Division
West Bethesda, MD 20817-5700

NSWCCD-CISD–2010/015 September 2010
Center for Innovation in Ship Design
Technical Report

DUKW-21 Autonomous Navigation: Transitioning Between Sea and Land

By
Benjamin D. Flom

NSWCCD-CISD-2010/015

REPORT DOCUMENTATION PAGE

Form Approved
OMB No. 0704-0188

1. REPORT DATE *(DD-MM-YYYY)*	**2. REPORT TYPE**	**3. DATES COVERED** *(From - To)*
01-09-2010	Final	24-05-2010 to 30-07-2010

4. TITLE AND SUBTITLE
DUKW-21 Autonomous Navigation: Transitioning Between Sea and Land

5a. CONTRACT NUMBER

5b. GRANT NUMBER

5c. PROGRAM ELEMENT NUMBER

6. AUTHOR(S)
Benjamin D. Flom

5d. PROJECT NUMBER

5e. TASK NUMBER

5f. WORK UNIT NUMBER

7. PERFORMING ORGANIZATION NAME(S) AND ADDRESS(ES) AND ADDRESS(ES)
Naval Surface Warfare Center
Carderock Division
9500 Macarthur Boulevard
West Bethesda, MD 20817-5700

8. PERFORMING ORGANIZATION REPORT NUMBER
NSWCCD-CISD-2010/015

9. SPONSORING / MONITORING AGENCY NAME(S) AND ADDRESS(ES)
Chief of Naval Research
One Liberty Center
875 North Randolph Street,
Suite 1425
Arlington, VA 22203-1995

10. SPONSOR/MONITOR'S ACRONYM(S)

11. SPONSOR/MONITOR'S REPORT NUMBER(S)

12. DISTRIBUTION / AVAILABILITY STATEMENT
Approved for Public Release: Distribution Unlimited

13. SUPPLEMENTARY NOTES

14. ABSTRACT

Autonomous amphibious vehicles have the potential to revolutionize supply chain operations involving the transport of cargo from a Sea Base to troops ashore. In 2007, a team of Center for Innovation in Ship Design (CISD) interns developed a design concept called DUKW-21, an amphibious vehicle meant to support one crew member onboard, with the potential for future integration of an autonomous control system. While DUKW-21 is designed to be a tracked vehicle, for simplicity, a wheeled 1/7th scale model was designed and built, called DUKW-ling, which has successfully demonstrated limited autonomy.

Unlike an air-cushion vehicle, a tracked or wheeled amphibious vehicle must travel through three distinct environments: sea, (dry) land, and the transition zone, where the vehicle's ground propulsors are engaged with the sea-floor, but the vehicle is still partially submerged underwater. In this report, an original, baseline model of a tracked or wheeled amphibious vehicle in the transition is developed. This model is then used to study vehicle routing in the transition with the objective of minimizing travel time. In particular, a closed-form characterization of a preferred travel route is derived. Under certain conditions, it is also shown that the baseline model of the transition can be applied to hills on land.

15. SUBJECT TERMS

16. SECURITY CLASSIFICATION OF:			**17. LIMITATION OF ABSTRACT**	**18. NUMBER OF PAGES**	**19a. NAME OF RESPONSIBLE PERSON**
					Colen Kennell
a. REPORT	**b. ABSTRACT**	**c. THIS PAGE**			**19b. TELEPHONE NUMBER** *(include area code)*
UNCLASSIFIED	UNCLASSIFIED	UNCLASSIFIED	UL	41	301-227-5468

Abstract

Autonomous amphibious vehicles have the potential to revolutionize supply chain operations involving the transport of cargo from a Sea Base to troops ashore. In 2007, a team of Center for Innovation in Ship Design (CISD) interns developed a design concept called DUKW-21, an amphibious vehicle meant to support one crew member onboard, with the potential for future integration of an autonomous control system. While DUKW-21 is designed to be a tracked vehicle, for simplicity, a wheeled 1/7th scale model was designed and built, called DUKW-ling, which has successfully demonstrated limited autonomy.

Unlike an air-cushion vehicle, a tracked or wheeled amphibious vehicle must travel through three distinct environments: sea, (dry) land, and the transition zone, where the vehicle's ground propulsors are engaged with the sea-floor, but the vehicle is still partially submerged underwater. In this report, an original, baseline model of the dynamics of a tracked or wheeled amphibious vehicle in the transition is developed. This model is then used to study vehicle routing in the transition with the objective of minimizing travel time. In particular, a closed-form characterization of a preferred travel route is derived. Under certain conditions, it is also shown that the baseline model of the transition can be applied to hills on land.

Acknowledgements

This report is the culmination of work conducted by a University of Maryland undergraduate student under the Naval Research Enterprise Intern Program sponsored by the Office of Naval Research. The work was performed in the Center for Innovation in Ship Design (CISD), which is part of the Ship Systems Integration and Design Department at Naval Surface Warfare Center Carderock Division. Acknowledged are several individuals that have been of great assistance in the development of this project:

Prof. Irina Dolinskaya of Northwestern University provided major technical guidance throughout the project, without which, this work would not be possible. Prof. Dolinskaya's significant contribution to this effort is especially acknowledged.

A variety of CISD personnel, staff and intern, have assisted this project. In particular, Mr. Max Harper, Mr. Jack Offutt, Dr. Colen Kennel, and Mr. Steven Ouimette have been of great support.

Table of Contents

List of Figures

Introduction

Background

The United States military currently relies heavily on large transport vessels part of the Maritime Pre-positioning Force (MPF), and developed deep water port facilities to deliver logistic material abroad. The difficulties in finding and securing port facilities in hostile areas spurred the development of the Sea Base concept; the provision of mobile port facilities in controlled waters. The key challenge to the concept is the development of a supply chain to transport cargo from the Sea Base to shore. One approach is to use a medium size container ship to transport cargo from the Sea Base to a location near the shore, at which point amphibious vehicles can run continuous delivery missions to a target location inland.

Automating the amphibious vehicles in such an application would have significant advantages. Having the capability for a team of unmanned amphibious vehicles to deliver cargo would free up the service crew for other tasks. In addition, unmanned vehicles can maneuver in more agile ways unconstrained by the acceleration limits that humans can tolerate, which would greatly increase the efficiency of the cargo transport supply chain. The Center for Innovation in Ship Design (CISD), a part of the Naval Surface Warfare Center Carderock Division, has been developing a concept for such an amphibious vehicle, called DUKW-21, shown in Figure 1.

In 2007, a team of CISD interns developed a design concept for DUKW-21, a tracked amphibious vehicle with a human support system for a single crew member that would facilitate the eventual implementation of an autonomous control system (Gonzalez et. al., 2007). Research into automating DUKW-21 started in 2009, when a CISD intern investigated existing ground and sea navigation algorithms and ways of integrating the different operational modes (Flom, 2009).

While DUKW-21 is designed to be a tracked vehicle, for simplicity, a wheeled $1/7^{th}$ scale model was developed, called DUKW-ling, which has successfully demonstrated limited autonomy (FAU, 2010). In this report, several issues associated with a tracked or wheeled amphibious vehicle driving up the sea-floor during the beaching phase are studied with the idea that in the future, the tools developed here can be tested on DUKW-ling.

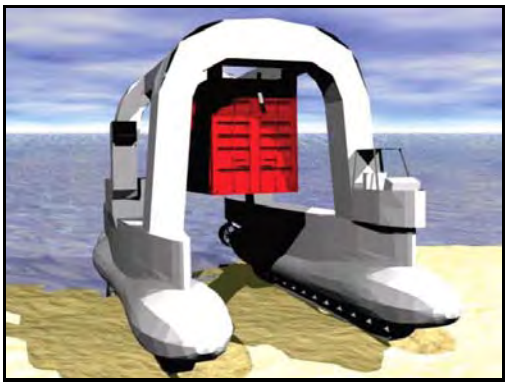

Figure 1: CISD DUKW-21 concept, borrowed from (Gonzalez et. al., 2007)

Challenges

Unlike an air-cushion vehicle, a wheeled/tracked amphibious vehicle must travel through three distinct environments: sea, (dry) land, and the transition zone, where in the transition, the vehicle's ground propulsors are engaged with the sea-floor, while the vehicle is still partially submerged in the water, as shown in Figure 2. We call the border between the sea and transition the engage line and the border between the transition and land the shoreline. All these terms are defined more precisely later.

Aside from additional hydrodynamic forces acting on the vehicle, there are a few characteristics that make the transition distinct from dry land. Firstly, the tire/track to ground surface friction coefficient is generally much smaller on sand submerged underwater than on dry land, which leads to a significantly smaller propulsive force that the vehicle can generate in the transition. This makes optimizing the route the vehicle follows critical because poor route planning can result in the vehicle being immobilized in wet sand, which would increase the time it takes for the vehicle to complete its mission, thereby delaying delivery of the supplies that the vehicle is transporting.

Another factor which makes the transition distinct from land is that the effective weight of the vehicle is not constant due to the change in buoyancy as the vehicle surfaces. This implies that existing navigation algorithms for ground vehicles are not necessarily applicable because they usually assume that the weight of the vehicle is constant.

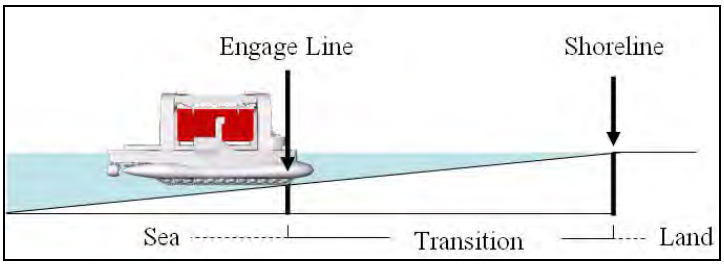

Figure 2: Amphibious operating environments

Report Overview

We make several contributions in this report. In the “Physical Model of Transition” chapter, we propose a baseline model for the transition. Then in the “Implications” chapter, the model is used to study vehicle routing, also known as trajectory or path-planning. It is also shown that under certain conditions, the proposed model can be used for navigating general hills on dry land. This extends the application of our research from autonomous amphibious vehicles to autonomous ground vehicles. Finally, in the “Discussion” chapter, we add intuition to our results, as well as state the existence of two interesting bounds. Finally, in the “Conclusion” chapter, we conclude with recommendations for future research.

Note, in the baseline model developed in “Physical Model of Transition,” wave and current forces are initially ignored. As no model currently exists for the transition that can facilitate real-time decision making by an autonomous agent, the main focus of this project was to develop a simplified model for initial analysis that in the future could be expanded and refined with the addition of a more comprehensive set of parameters.

Preliminaries

Chapter Overview

In this chapter, we establish terminology and develop a coordinate system that will be used in the development of the model in the next chapter. We follow with a precise definition of the problem statement. Then, to motivate our work, we briefly review the existing literature and discuss their limitations as they apply to our problem.

Terminology

We define the map $\mathbb{M} \subset \mathbb{R}^2$ to be the set of all planar points where the vehicle's center of mass could be positioned. Define a terrain elevation function $E : \mathbb{M} \to \mathbb{R}$, such that when the vehicle's center of mass is at $\mathbf{w} \in \mathbb{M}$, the elevation of the ground surface or sea floor at **w** is *E*(**w**) relative to the sea-level.

Define a draft function $h : \mathbb{M} \to \mathbb{R}_+ \cup \{0\}$ such that when the vehicle's center of mass is at **w**, the draft, or vertical distance from the waterline to the bottom of the hull, is *h*(**w**). Let H be the maximum draft of the vehicle (corresponding to a floating vehicle at sea).

Now define the world $\mathbb{W}$ to be the surface in $\mathbb{R}^3$ that denotes the position of the bottom of the vehicle's wheels/tracks. More precisely,

$$\mathbb{W} := \{(x, y, z) \in \mathbb{R}^3 \mid (x, y) \in \mathbb{M},\ z = \max\{E((x, y)), -H\} \text{ if } E((x, y)) < 0,\ z = E((x, y)) \text{ if } E((x, y)) \geq 0\}.$$

The operating environments are now precisely defined. We define the sea $S := \{(x, y, z) \in \mathbb{W} \mid h((x, y)) = H\}$; the land, $L := \{(x, y, z) \in \mathbb{W} \mid h((x, y)) = 0\}$; and the transition $T_0 := \{(x, y, z) \in \mathbb{W} \mid h((x, y)) \in (0, H)\}$. For our analysis, we consider the closure of T_0, denoted $T := \bar{T}_0$. Next the borders are defined.

The engage line, $l_e := \bar{S} \cap T$, where $\bar{S}$ is the closure of *S*. Likewise, the shoreline, $l_s := L \cap T$. See Figure 3 for an illustration of the engage line and shoreline relative to the transition. Then, our first baseline assumption is made:

Assumption 1. The engage line, l_e, and shoreline, l_s, are straight lines and parallel to each other.

Without loss of generality, we orient the coordinate system such that $l_e = \{(x, y, z) \in \mathbb{W} \mid y = 0\}$. Define the distance between the engage line and the shoreline:

$$Y := \min_{(x_1,y_1,z_1)\in l_e,\ (x_2,y_2,z_2)\in l_s} ||(x_2,y_2)-(x_1,y_1)||,$$

where $||\cdot||$ is the Euclidean norm. The direction from the engage line to the shoreline is defined to be the positive y-axis direction. That is, $l_s = \{(x,y,z) \in \mathbb{W} \mid y = Y\}$

Another baseline assumption is made:

Assumption 2. The sea-floor is planar in the closure of the transition. That is, for $A := \{(x,y) \in \mathbb{M} \mid (x,y,E((x,y))) \in T\}$, $E : A \to \mathbb{R}$ is affine, i.e., $\exists\ \sigma > 0\ st\ \forall\ (x,y,z) \in T$ and $\forall\ y_1 \in [0,Y),\ y_2 \in (y_1,Y],\ \frac{E(x,y_1)-E(x,y_2)}{y_2-y_1} = \sigma.$

Define $\alpha \in [0, \frac{\pi}{2})$ to be the angle of inclination of the sea-floor in the transition. That is, $\alpha := \tan^{-1}(\sigma)$. See Figure 3 and Figure 4 for an illustration of the transition with Assumptions 1 and 2.

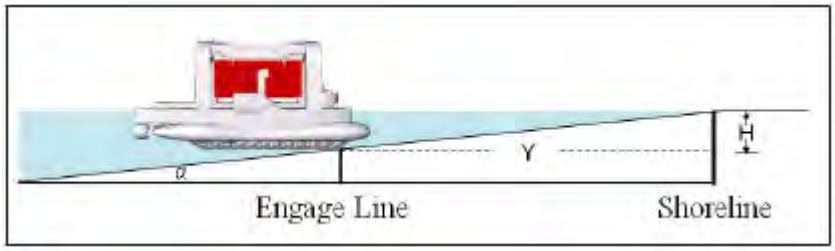

Figure 3: Sideview of transition with Assumptions 1 and 2

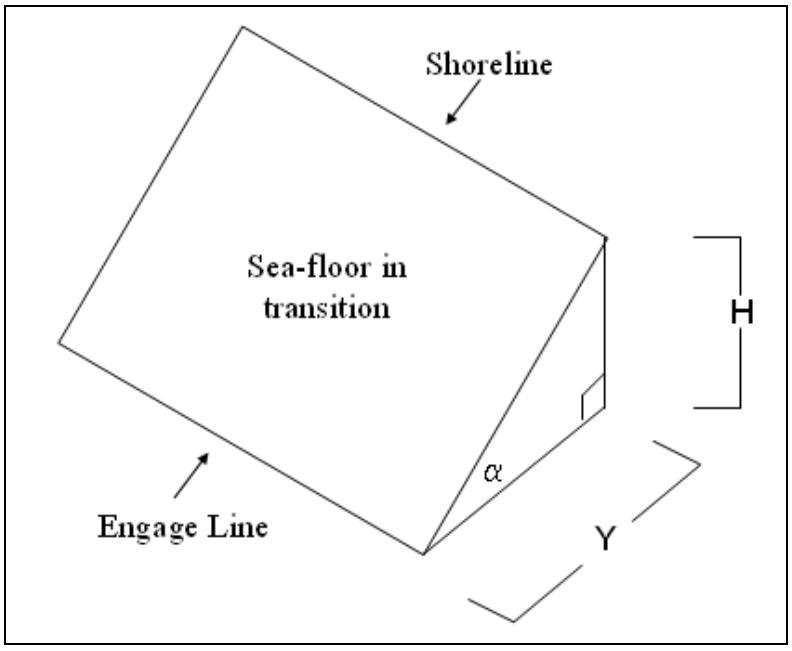

Figure 4: Isometric view of transition with Assumptions 1 and 2

Established Coordinate System

In this section, a precise coordinate system is defined for the analysis that will take place later. Recall that a point in *T* is an ordered triplet. In the previous section, we implicitly considered a coordinate system {x,y,z} as illustrated in Figure 5. For example, the elevation function maps a point in the {x,y} plane to the z-axis. This coordinate system was only used to allow for intuitive definitions of the vehicle's operating environments. We now introduce the transformed coordinate system that will be used for the remainder of the paper.

Following from Assumption 2, the vehicle maneuvers in the plane that intersects the shoreline and the engage line as depicted in Figure 3 and Figure 4. To allow most of our analysis to be performed in two dimensions rather than three, we define a new coordinate system $\{\tilde{x}, \tilde{y}, \tilde{z}\}$ which is the {x,y,z} coordinate system rotated about the shoreline by $\frac{\pi}{2} - \alpha$, and translated in the $-\tilde{y}$ direction such that the $\tilde{x}$-axis corresponds to the engage line, as shown in Figure 6. Define the unit vectors $\tilde{\mathbf{i}}, \tilde{\mathbf{j}}$, and $\tilde{\mathbf{k}}$ corresponding to the $\tilde{x}$, $\tilde{y}$, and $\tilde{z}$ axis, respectively.

We define the sea-floor plane, denoted $\tilde{T}$, as the closure of the transition rotated about the shoreline as is done for the $\{\tilde{x}, \tilde{y}, \tilde{z}\}$ coordinate system. That is, $\tilde{T} := \{(\tilde{x}, \tilde{y}, 0) \in \mathbb{R}^3 \mid (\tilde{x}, \tilde{y}\cos\alpha, 0) \in T\}$. Similarly, define $\tilde{Y} := \frac{Y}{\cos\alpha}$ to obtain the distance between the engage line and shoreline *with respect to the sea-floor plane.* From this point on, we always refer to the $\{\tilde{x}, \tilde{y}, \tilde{z}\}$ coordinate system.

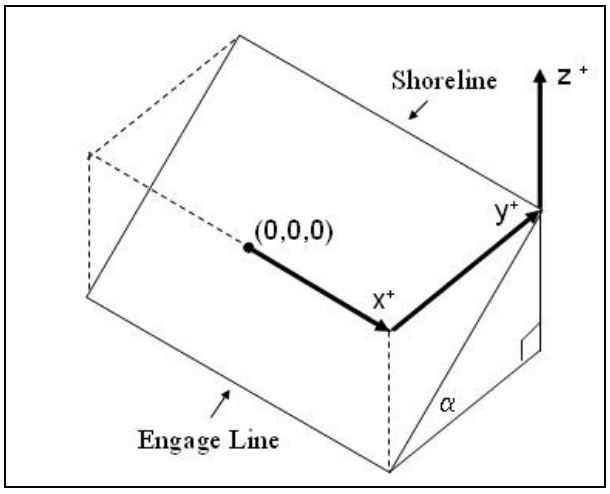

Figure 5: Position coordinate system

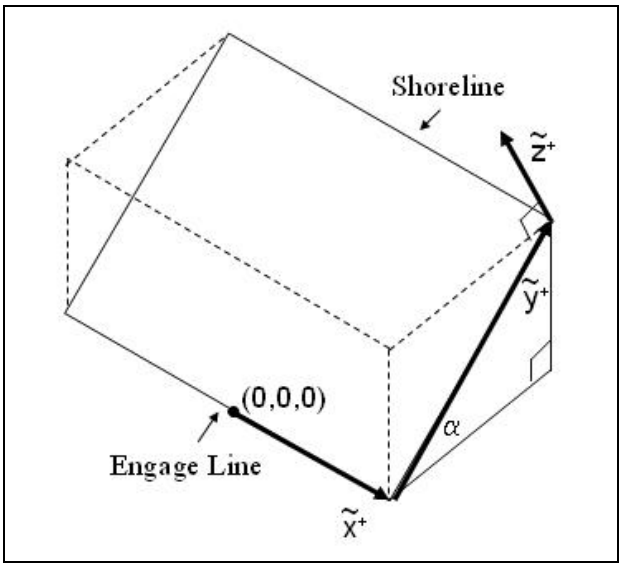

Figure 6: Force coordinate system

In this analysis, we consider the vehicle's heading angle, denoted θ, which is measured relative to the positive $\tilde{x}$-axis. As illustrated in Figure 7, a heading angle of 0 corresponds to traveling parallel to the engage line and the shoreline, and a heading angle of $\pi/2$ radians corresponds to traveling perpendicular towards the shoreline.

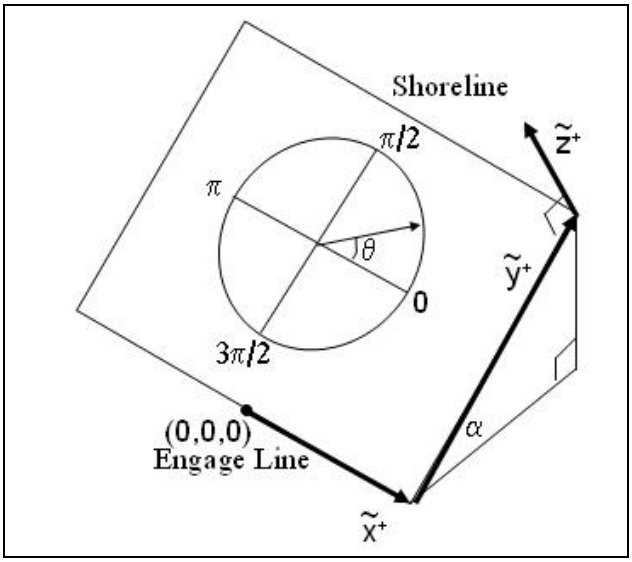

Figure 7: Heading angle θ with respect to sea-floor plane

A final remark about notation. A symbol denoted with a bold letter, such as a position-dependent force **F**, always represents a vector in $\mathbb{R}^3$, (i.e., $\boldsymbol{F} : \tilde{T} \rightarrow \mathbb{R}^3$), and a symbol not in bold which has a corresponding bold symbol, such as F,

represents the magnitude of the corresponding bold faced force. That is F(**w**) := ||**F(w)**||, $\forall$ **w** $\in \tilde{T}$.

Problem Statement

Before presenting the problem statement, we first provide some context. When a wheel or tracked amphibious vehicle makes contact with the engage line, a significant amount of energy is lost in the system. Hence, the vehicle effectively starts from near rest when it begins its journey to the shoreline from the engage line.

Furthermore, as discussed earlier, the tire/track to ground surface friction coefficient is very small, which would result in significant tire/track slipping, making maneuvering a major challenge. It may be most practical to implement a traction control system on the vehicle, which would keep the tires/tracks rotating at the speed that would maximize the tractive force generated by the vehicle. In this case, linear paths in the transition are preferred. Now a formal statement of the problem is given, with an accompanying illustration in Figure 8.

Problem statement: Let the vehicle start at position $(0,0,0) \in l_e$ with heading angle $\theta \in (0,\pi)$, initially at rest. Let $\mathbb{L}$ be the set of all line segments, or linear paths, connecting (0,0,0) to points on l_s. That is, $\forall\ l \in \mathbb{L},\ \exists\ (\tilde{x}_1, \tilde{y}_1, 0) \in l_s,\ \lambda \in \mathbb{R}\ \ st\ \forall\ \tilde{x} \in [0, \tilde{x}_1],\ (\tilde{x}, \lambda\tilde{x}, 0) \in l$. Denote the time it takes to travel from (0,0,0) to l_s along a linear path $l \in \mathbb{L},\ t(l)$. Our objective is to find $\underset{l \in \mathbb{L}}{\operatorname{argmin}}\{t(l)\}$.

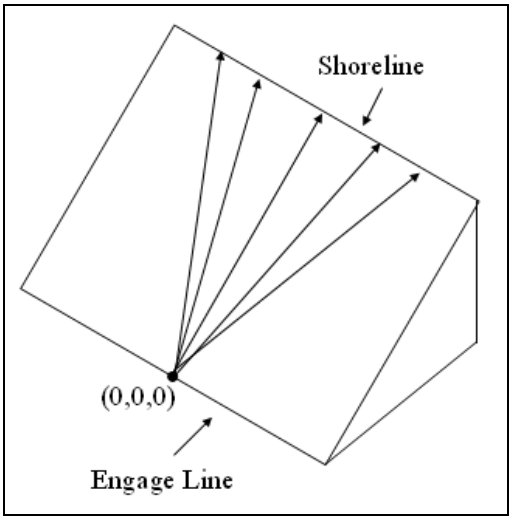

Figure 8: Set of linear trajectories from p on the engage line to the shoreline.

Related Work

To our knowledge, there has been no research on path planning for an amphibious vehicle in the transition. In particular, there is no existing physical model of the transition that has low enough complexity to facilitate the development of real-time path-planning algorithms for an autonomous agent to use. A widely used physical model for a general terrain on dry land is developed in (Rowe & Ross, 1990), and has been used to develop successful algorithms for autonomous navigation on dry land (Sun & Reif, 2005). In addition to not considering buoyancy, the models also neglect acceleration, and their objective is to minimize energy, whereas in the following analysis our objective is to minimize travel-time.

Physical Model of Transition

Forces Generated by and Acting on the Vehicle

In this section, we discuss the forces in the system consisting of the vehicle driving up the sea-floor in the transition. Recall that wave and current forces are neglected in this baseline model. Note, we assume that all forces are acting on the vehicle's center of mass.

The only considered force generated by the vehicle is the tractive force of the ground propulsors, denoted $\boldsymbol{F}_{trac} : \tilde{T} \to \mathbb{R}^3$. We assume that when the vehicle's wheels or tracks are engaged in the sea-floor, the efficiency of the waterborne propulsors will be negligible compared to the ground propulsion force and is omitted in our analysis. As discussed in (Gillespie, 1992), the principal forces acting on a vehicle driving up a sloped surface on land are the weight, the normal force, the rolling resistance, and the drag, denoted $\boldsymbol{W}, \boldsymbol{N}, \boldsymbol{R}_{rr}, \boldsymbol{D} : \tilde{T} \to \mathbb{R}^3$, respectively. In the transition, there is an additional force of buoyancy, denoted $\boldsymbol{B} : \tilde{T} \to \mathbb{R}^3$. A side-view of the force diagram in the transition is shown in Figure 9.

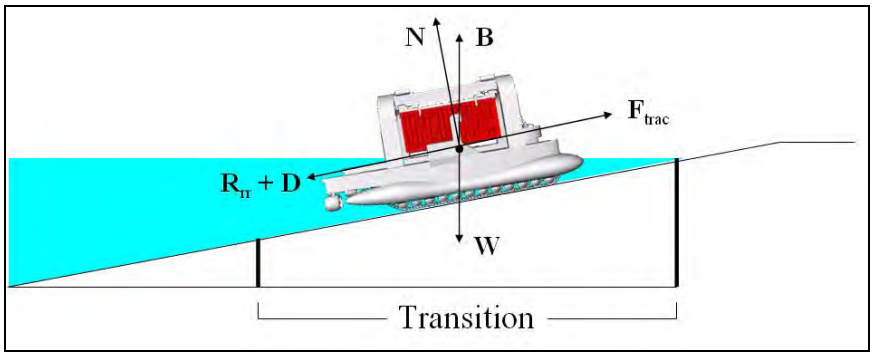

Figure 9: Forces generated by, or acting on the vehicle in the transition

Before we begin the analysis of the transition forces, we establish consistent notation to precisely describe the vehicle's effective weight. We define the weight **W** := m**g**, where m is the vehicle's mass and **g** is the gravitational acceleration. Define the effective weight, $\mathbf{W}_e$:=**W** + **B** (where W_e = W - B). The effective weight can be split into the effective normal weight, denoted W_{en}, and the effective tangential weight, denoted W_{et}, where $W_{en} = W_e \cos\alpha$ and $W_{et} = W_e \sin\alpha$, as shown in Figure 10. Note that **N** + $\mathbf{W}_{en}$ = **0**.

It then follows that $R_{rr} = c_{rr}W_{en}$, where c_{rr} is the rolling resistance coefficient between the tires/tracks and the ground surface (Gillespie, 1992).

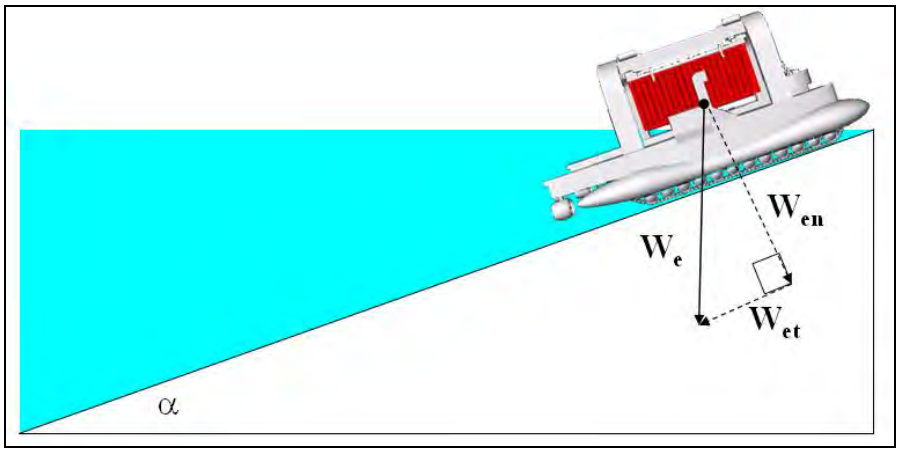

Figure 10: Effective weight (W_e) split into normal (W_{en}) and tangential (W_{et})

Vehicle Traveling Perpendicular to the Shoreline

In this section, we consider in more detail, the forces generated by, and acting on, the vehicle as it drives up the sea-floor plane in a straight line perpendicular to the shoreline and engage line (that is, $\theta = \pi/2$). A more general discussion for arbitrary heading is presented in the next section. The following assumption is made:

Assumption 3. The net force is always positive in the positive $\tilde{y}$ direction. That is, the vehicle can always overcome resistance and opposing forces to move forward/towards the shore.

The net force of a ground vehicle driving perpendicularly up a hill with an incline of angle α is usually modeled with Equations (1) – (3) (Gillespie, 1992). See Figure 11 for an illustration of the sea-floor planar forces in the transition.

$$\mathbf{F} = \mathbf{F}_{trac} + \mathbf{W}_{et} + \mathbf{R}_{rr} + \mathbf{D}, \tag{1}$$

$$F = F_{trac} - W_{et} - R_{rr} - D, \tag{2}$$

$$\mathbf{F} = F\tilde{\mathbf{j}} \tag{3}$$

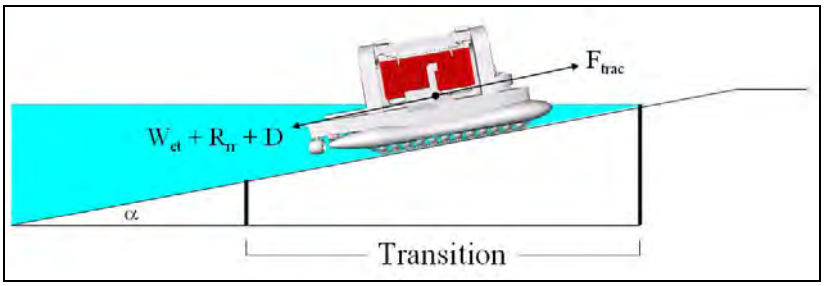

Figure 11: Sea-floor planar forces in the transition

Since our goal is to find the linear path that minimizes travel time, without loss of optimality we assume that the tractive force generated by the vehicle is equal to the maximum tractive force it can generate. Hence, for the remainder of the paper, we will replace F_{trac} with F_{MTr}, which is defined as the maximum tractive force.

We now review a commonly used model for obtaining the maximum tractive force a ground vehicle can generate, as described in (Gillespie, 1992). In general, there are two classes of properties that can limit the maximum tractive force. The first is engine and drivetrain characteristics, including engine torque, gear ratios, efficiency of the drive system, and the inertia of the engine and drivetrain components. When this class limits the maximum tractive force, the expression is:

$$F_{MTr1} = \frac{T_e N_{tf} \eta_{tf}}{r} - \left((I_e + I_t)N_{tf}^2 + I_d N_f^2 + I_w\right)\frac{a}{r^2}, \qquad (4)$$

where:

F_{MTr1} is the maximum tractive force the vehicle can generate when the upper bound is caused by the first class of properties

T_e is the maximum engine torque

N_{tf} is the combined ratio of transmission and final drive

η_{tf} is the combined efficiency of transmission and final drive

r is the radius of the wheels

I_e is the engine rotational inertia

I_t is the rotational inertia of the transmission as seen from the engine side

I_d is the rotational inertia of the driveshaft

N_f is the numerical ratio of the final drive

I_w is the rotational inertia of the wheels and axle shafts

a is the acceleration of the vehicle

Equation (4) accurately characterizes the maximum tractive force for large friction coefficients. For small friction coefficients between the tire and the road, the maximum tractive force is:

$$F_{MTr2} = \mu_f W_e, \tag{5}$$

where μ_f is the peak friction coefficient. We now demonstrate the similarities in the structures of F_{MTr1} and F_{MTr2}. Introduce the constants:

$$\begin{aligned} b_1 &:= \frac{T_e N_{tf} \eta_{tf}}{r} \\ b_2 &:= \frac{(I_e + I_t) N_{tf}^2 + I_d N_f^2 + I_w}{r^2} \end{aligned}$$

Rewrite Equations (4) and (5) as follows:

$$\begin{aligned} F_{MTr1} &= \frac{b_1}{W_e} * W_e - b_2 a \\ F_{MTr2} &= \mu_f W_e - 0a \end{aligned} \tag{6}$$

Then, the general maximum tractive force the vehicle can generate can be written as:

$$F_{MTr} = \mu W_e - \gamma a, \tag{7}$$

where:

$$\mu = \begin{cases} \frac{b_1}{W_e} & F_{MTr1} < F_{MTr2} \\ \mu_f & F_{MTr1} \geq F_{MTr2} \end{cases}$$

and:

$$\gamma = \begin{cases} b_2 & F_{MTr1} < F_{MTr2} \\ 0 & F_{MTr1} \geq F_{MTr2} \end{cases}$$

An assumption is stated:

Assumption 4. The track/sea-floor peak friction coefficient μ_f and the track/sea-floor rolling resistance coefficient c_{rr} are constant throughout the transition. It follows that μ is constant throughout the transition.

When the vehicle travels towards the shoreline from the engage line, and the heading is perpendicular to the shoreline, it follows:

$$\mathbf{F}_{MTr} = (\mu W_e - \gamma a)\tilde{\mathbf{j}} = (\mu(W - B) - \gamma a)\tilde{\mathbf{j}} = [\mu(mg - \rho g V_{disp}) - \gamma a]\tilde{\mathbf{j}}, \quad (8)$$

where F_{MTr} is the maximum tractive force, ρ is the fluid density, and V_{disp} is the volume of displaced fluid.

Moreover:

$$\begin{aligned} \mathbf{R}_{rr} &= -c_{rr} W_{en}\tilde{\mathbf{j}} = -c_{rr}(W - B)\cos\alpha\tilde{\mathbf{j}} \\ &= -c_{rr}\cos\alpha(mg - \rho g V_{disp})\tilde{\mathbf{j}}, \end{aligned} \quad (9)$$

Integrating drag into the model significantly increases the complexity. Because of the expected slow speeds that the vehicle can travel at in the transition, it was decided that drag, which is proportional to the speed squared, would be small relative to other forces, and hence, can be neglected in the initial analysis. In the future, we plan on studying ways of integrating drag into our model and relaxing the following assumption:

Assumption 5. Drag is negligible in the transition.

We couple the maximum tractive force with the rolling resistance by defining the maximum relative ground propulsive force, $\mathbf{F}_{MG} := \mathbf{F}_{MTr} + \mathbf{R}_{rr} \Rightarrow F_{MG} = F_{MTr} - R_{rr}$. Substituting in Equations (8) and (9) yields:

$$\mathbf{F}_{MG} = [(\mu - c_{rr}\cos\alpha)(mg - \rho g V_{disp}) - \gamma a]\tilde{\mathbf{j}}. \quad (10)$$

In general, precisely calculating the volume of displaced water when the vehicle surfaces is very challenging, and requires intricate knowledge of the hull form. Assuming that the volume of displaced fluid is a linear function of the depth of the hull greatly decreases the complexity of the problem, so for now we make Assumption 6. In the future we will study ways of approximating the hull form piecewise linearly.

Assumption 6. The volume of displaced fluid is a linear function of the draft, or vertical distance from the waterline to the bottom of the hull.

Let V_H be the maximum displaced volume, corresponding to when the draft equals *H*. By Assumption 6, the displaced volume at a draft *h* is equal to $\frac{h}{H}V_H$. We can now extend Equation (10) to express it as a function of the draft:

$$F_{MG}(h) = (\mu - c_{rr}\cos\alpha)mg - \gamma a - (\mu - c_{rr}\cos\alpha)g\rho\frac{V_H}{H}h. \qquad (11)$$

In order to model the propulsive forces as a function of the vehicles position in the sea-floor plane, we replace the draft variable *h* with the variable $\tilde{y}$, corresponding to sea-floor planar distance from the engage line. As can be seen in Figure 12, $h = (\tilde{Y} - \tilde{y})\sin\alpha,$ so Equation (11) can be replaced with:

$$\begin{aligned} F_{MG}(\tilde{y}) &= (\mu - c_{rr}\cos\alpha)mg - \gamma a - (\mu - c_{rr}\cos\alpha)g\rho\frac{V_H}{H}\sin(\alpha)(\tilde{Y} - \tilde{y}) \\ &= (\mu - c_{rr}\cos\alpha)mg - (\mu - c_{rr}\cos\alpha)g\rho\frac{V_H}{H}\sin(\alpha)\tilde{Y} - \gamma a \\ &\quad +(\mu - c_{rr}\cos\alpha)g\rho\frac{V_H}{H}\sin(\alpha)\tilde{y} \qquad (12) \end{aligned}$$

Introducing the constants
$a_1 := (\mu - c_{rr}\cos\alpha)mg - (\mu - c_{rr}\cos\alpha)g\rho\frac{V_H}{H}\sin(\alpha)\tilde{Y}$ and
$a_2 := (\mu - c_{rr}\cos\alpha)g\rho\frac{V_H}{H}\sin\alpha,$ we deliver a more elegant form of Equation (12),

$$F_{MG}(\tilde{y}) = a_1 + a_2\tilde{y} - \gamma a \qquad (13)$$

where $\mathbf{F}_{MG}(\tilde{y}) = F_{MG}(\tilde{y})\tilde{\mathbf{j}}.$

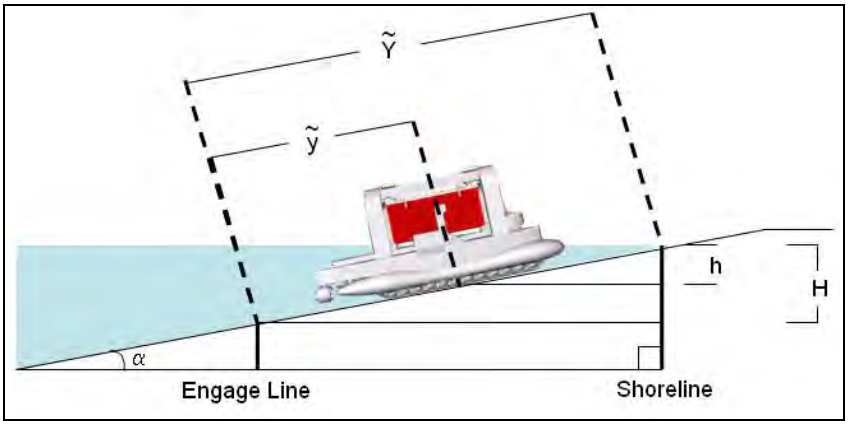

Figure 12: Transition with distance variables

To review, Equation (13) characterizes the sum of F_{trac} (= F_{MTr}) and R_{rr} as in Equation (1). Based on Assumption 5, we omit the drag force (D) from Equation (1). Lastly, we integrate the effective tangential weight. Recall,

$$W_{et}(h) = W_e \sin\alpha = (W - B)\sin\alpha = (mg - \rho g \frac{V_H}{H} h)\sin\alpha \qquad (14)$$

Making the $h = (\tilde{Y} - \tilde{y})\sin\alpha$ substitution delivers,

$$W_{et}(\tilde{y}) = (mg\sin\alpha - \rho g \frac{V_H}{H}(\sin\alpha)^2 \tilde{Y}) + \rho g \frac{V_H}{H}(\sin\alpha)^2 \tilde{y}. \qquad (15)$$

Setting the constants: $p_1 := mg\sin\alpha - \rho g \frac{V_H}{H}(\sin\alpha)^2 \tilde{Y}$ and $p_2 = \rho g \frac{V_H}{H}(\sin\alpha)^2$ yields,

$$W_{et}(\tilde{y}) = p_1 + p_2 y,\ p_1, p_2 \in \mathbb{R}, \qquad (16)$$

where $\mathbf{W}_{et}(\tilde{y}) = -W_{et}(\tilde{y})\tilde{\mathbf{j}}$.

To combine all the discussions together, we define the maximum net force when the vehicle's heading is perpendicular to the shoreline, $\mathbf{F}_{max} := \mathbf{F}_{MG} + \mathbf{W}_{et}$, where $F_{max} = F_{MG} - W_{et}$, which we can express precisely as a function of the beach planar distance from the engage line ($\tilde{y}$) and the acceleration (a):

$$F_{max}(\tilde{y}) = (a_1 + a_2\tilde{y}) - (p_1 + p_2\tilde{y}) - \gamma a, \qquad (17)$$

where $\mathbf{F}_{max}(\tilde{y}) = F_{max}(\tilde{y})\tilde{\mathbf{j}},$ following from Assumption 3.

Traveling towards Shoreline with Arbitrary Heading

Up to this point, we have only considered forces as the vehicle drives towards the shoreline in a straight, perpendicular fashion. We now add to our analysis the vehicle's heading angle, θ, and extend our discussion to the vehicle traveling at a non-normal angle relative to the shoreline, as shown in Figure 12. In this section, we consider the forces generated by, and acting on, the vehicle when it has a heading angle strictly between 0 and π. In other words, only the case when the vehicle is driving towards the shoreline is considered in this analysis.

Equation (17) is not direction-dependent because it follows from Equation (1), which assumes the vehicle is traveling perpendicular to the shoreline. Another way to interpret this is that $\mathbf{W}_{et}$ was assumed to be acting on the vehicle parallel to the direction of wheel/track rotation. When $\theta \neq \frac{\pi}{2}$, part of $\mathbf{W}_{et}$ acts on the vehicle perpendicular to the direction of wheel/track rotation, which has a different effect. $\mathbf{W}_{et}$ can be characterized as a sum of a vector normal to the vehicle's heading direction, denoted $\mathbf{W}_{etn}$, and a vector tangent to the vehicle's heading direction, denoted $\mathbf{W}_{ett}$, both also contained in the sea-surface plane, as

illustrated in Figure 13. Using trigonometry, it can be shown that $W_{ett} = W_{et} \sin\theta$ and $W_{ent} = W_{et} \cos\theta$.

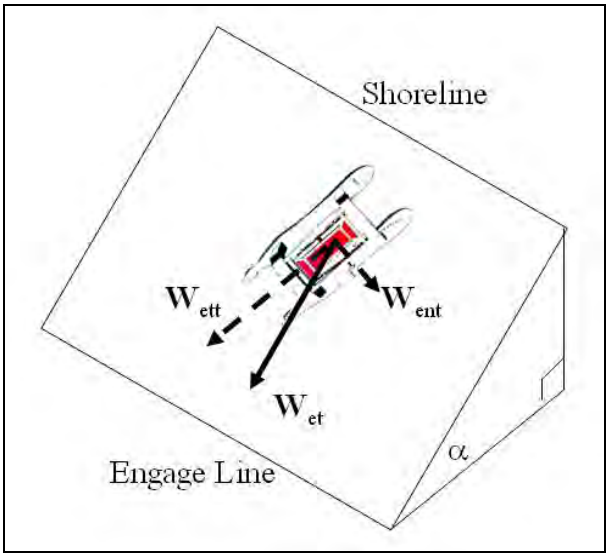

Figure 13: Effective tangential weight split into vector components in sea-floor plane

$\mathbf{W}_{ent}$ causes a collinear resistance force, $\mathbf{R}_s$ in the opposite direction, which takes into account sideways friction of the tracks. Tracks typically dig into the soil, which makes it even harder for a vehicle to slide sideways. Hence, we make the following assumption:

Assumption 7. The vehicle cannot slide sideways in the transition as a result of gravity. That is, $\mathbf{R}_s = -\mathbf{W}_{ent}$. See Figure 14 for an illustration of this assumption.

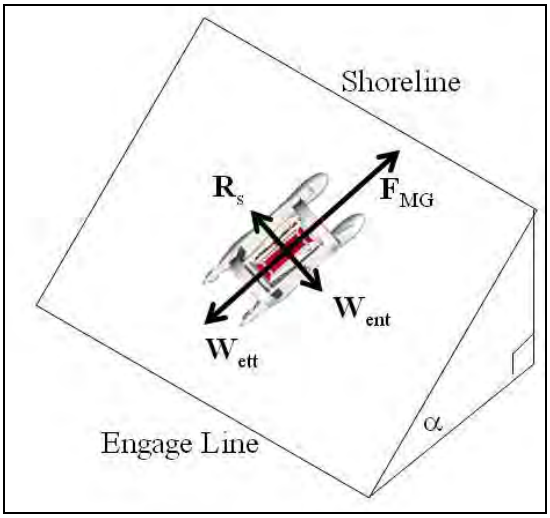

Figure 14: Sea-floor planar force diagram with Assumption 7

To review, we replaced $\mathbf{W}_{et}$ with $\mathbf{W}_{ett}$ in Equation (1). Applying a similar analysis as in the previous section, we can extend Equation (13) to get a characterization of the maximum net force of the vehicle positioned at a point $(\tilde{x}, \tilde{y}) \in \tilde{T}$ and traveling at an arbitrary angle $\theta \in [0, \pi]$:

$$F_{max}(\tilde{x}, \tilde{y}, \theta) = (a_1 + a_2\tilde{y}) - (p_1 + p_2\tilde{y}) \sin\theta - \gamma a, \tag{18}$$

where $\mathbf{F}_{max}(\tilde{x}, \tilde{y}, \theta) = F_{max}(\tilde{x}, \tilde{y}, \theta)(\cos\theta\tilde{\mathbf{i}} + \sin\theta\tilde{\mathbf{j}})$.

To solve for the maximum acceleration, set $F_{max} = ma \Rightarrow$:

$$a(\tilde{x}, \tilde{y}, \theta) = \frac{(a_1 + a_2\tilde{y}) - (p_1 + p_2\tilde{y}) \sin\theta}{m + \gamma} \tag{19}$$

Defining the constants: $\hat{a}_1 := \frac{a_1}{m+\gamma}, \hat{a}_2 := \frac{a_2}{m+\gamma}, \hat{p}_1 := \frac{p_1}{m+\gamma}, \hat{p}_2 := \frac{p_2}{m+\gamma}$, we get a characterization of the maximum acceleration of the vehicle positioned at $(\tilde{x}, \tilde{y})$ traveling at an arbitrary heading angle θ:

$$a_{max}(\tilde{x}, \tilde{y}, \theta) = (\hat{a}_1 + \hat{a}_2\tilde{y}) - (\hat{p}_1 + \hat{p}_2\tilde{y}) \sin\theta \tag{20}$$

Implications/Analysis of the Force Model

Chapter Overview

In this chapter, we first consider the problem of finding the linear path connecting an initial starting position on the engage line to the shoreline which minimizes travel time. This is an important problem to solve because the amphibious vehicle will be transporting supplies that are urgently needed ashore, such as food and medicine. Because of the low friction coefficient between the wheels/tracks and wet sand, the maximum propulsive force of the vehicle is significantly smaller in the transition than on dry land. Hence, traveling on a slower path has the potential to greatly increase the time needed to deliver supplies.

The results obtained for path planning in the transition, as we show, can be applied to hills on dry land in certain situations, which we discuss later in the chapter.

Note: all the proofs are omitted here and can be found in Appendix A.

Fastest Linear Path in Transition

In this section, we present the main contribution of this report, which is a closed form expression for the heading angle corresponding to the fastest linear path for a vehicle to travel from an initial starting point in the engage line that terminates at the shoreline. The expressions are stated in Theorems 5 and 9. From Assumption 7, we get Equation (20), which demonstrates how the maximum acceleration the vehicle can obtain is dependent on the heading angle of the traveling vehicle.

The critical step in finding the optimal heading angle is Lemma 1, which yields a closed form expression for the travel time along any linear path assuming the vehicle travels as fast as possible. The key to proving this lemma is to recognize that $\frac{\hat{a}_1}{\hat{a}_2} = \frac{\hat{p}_1}{\hat{p}_2}$, which we establish below.

Lemma 1. Let the vehicle start at position $(0,0,0) \in l_e$ with heading angle $\theta \in (0,\pi)$, initially at rest. Let *l* be a straight line segment along θ connecting (0,0,0) to a point $\left(\Delta\tilde{x}, \tilde{Y}, 0\right) \in l_s$, where $\Delta\tilde{x} = \frac{\tilde{Y}}{\tan\theta} > 0.$ Suppose Assumptions 1 through 7 hold, and that the vehicle will always travel as fast as possible. Also, assume that neither $\tilde{a}_2$ nor $\tilde{p}_2$ equals 0. Then, the travel time along line *l* is:

$$t(\lambda) = K\sqrt{\frac{1+\frac{1}{\lambda^2}}{\hat{a}_2\sqrt{1+\frac{1}{\lambda^2}}-\hat{p}_2}}, \tag{21}$$

Where $\lambda = \frac{\tilde{Y}}{\triangle\tilde{x}} = \tan\theta$, $K = \int_0^{\tilde{Y}} \frac{d\tilde{y}}{\sqrt{(\tilde{y}+k)^2-k^2}}$, and $k = \frac{\tilde{p}_1}{\tilde{a}_1} = \frac{\tilde{p}_2}{\tilde{a}_2}$.

The last hypothesis in Lemma 1, that neither $\tilde{p}_2$ nor $\tilde{a}_2$ equals 0, implies that the displaced water volume is nonzero, which means the vehicle is in the transition and not on dry land. Observe that if $\tilde{a}_2$ = 0, Equation (21) does not make sense. We could have weakened the hypothesis to just say $\tilde{a}_2 \neq 0$, however $\tilde{a}_2 = 0 \Rightarrow \tilde{p}_2 = 0$.

Theorem 2. Let the conditions in Lemma 1 hold. Further, assume that $\frac{\hat{p}_2}{\hat{a}_2} > \frac{1}{2}$. Then, the linear path which minimizes travel time corresponds to the vehicle traveling at angle:

$$\theta_* = \tan^{-1}\left(\sqrt{\frac{1}{4\left(\frac{\sin\alpha}{\mu-c_{rr}\cos\alpha}\right)^2-1}}\right) \tag{22}$$

To clarify the last hypothesis, observe that if $\frac{\hat{p}_2}{\hat{a}_2} = \frac{\sin\alpha}{\mu-c_{rr}\cos\alpha} \leq \frac{1}{2}$, Equation (32) does not make sense. Intuitively, this means that Theorem 2 is applicable when the friction coefficient between the tires/tracks and ground surface is sufficiently small and the rolling resistance coefficient is sufficiently large (such as on wet sand), and/or the slope of the sea-floor plane is sufficiently large.

We now present an example of a situation when Theorem 2 applies, that is, when $\frac{\hat{p}_2}{\hat{a}_2} > \frac{1}{2}$. Heavy trucks on sand generally encounter a rolling resistance coefficient of about 0.25, so assume c_{rr} = 0.25 (Gillespie, 1992). Further, wet tires can have friction coefficients of approximately 0.4, so assume μ = 0.4 (Jones & Childers, 2000). Now observe that when the sea-floor plane has an angle of α = 10°, $\frac{\hat{p}_2}{\hat{a}_2} = \frac{\sin\alpha}{\mu-c_{rr}\cos\alpha} = \frac{\sin 10}{0.4-0.25\cos 10} \approx 1.13 > \frac{1}{2}$.

Then, by Theorem 2, the optimal heading angle $\theta_* \approx 22^o$, which is noticeably different than the perpendicular heading angle of 90°.

Now we consider the case not covered by Theorem 2, that is, when $\frac{\hat{p}_2}{\hat{a}_2} \leq \frac{1}{2}$.

Theorem 3. Let the assumptions in Lemma 1 hold. Further, suppose that $\frac{\hat{p}_2}{\hat{a}_2} \leq \frac{1}{2}$. Then, the linear path which minimizes travel time is the normal line connecting (0,0,0) to l_s. That is, $\theta_* = \frac{\pi}{2}$.

Fastest Linear Path on Dry Hill

Observe that in Lemma 1, Theorem 2, and Theorem 3, it is assumed that $\hat{p}_2$ and $\hat{a}_2$ are not equal to zero. This makes sense when the vehicle is in the transition, and the displaced water volume is strictly greater than zero. However, as we show in this section, the final characterization of the optimal linear path in the transition does not depend on the effective weight. In other words, the buoyancy term cancels out, and our results can be extended to traveling on dry land. We demonstrate this in the remainder of the chapter.

Consider a vehicle travelling up a sloped terrain. Similarly to the definition of the closure of the transition, *T,* we define a *planar surface of a hill*, denoted by $\mathbb{H}$. $\mathbb{H}$ is assumed to be an affine two-dimensional surface with a inclination angle α, and contains the closure border lines: the *bottom line*, $l_b \subset \mathbb{H},$ and the *top line*, $l_t \subset \mathbb{H},$ analogous to l_e and l_s for *T*. Assumptions 1 through 4 and 7 are also extended to hold for $\mathbb{H}$.

Observe that for a planar surface of a hill, our discussion and results from the previous two chapter still hold, with the exception that now $V_H = 0$, which implies that $a_2 = \hat{a}_2 = p_2 = \hat{p}_2 = 0,$, and that $a_1 = (\mu - c_{rr}\cos\alpha)mg$ and $p_1 = mg\sin\alpha.$ The results are now stated.

Lemma 4. Let the vehicle start at position $(0,0,0) \in l_b$, with heading angle $\theta \in (0,\pi)$, initially at rest. Let *l* be a straight line segment along θ connecting (0,0,0) to a point $\left(\triangle\tilde{x}, \tilde{Y}, 0\right) \in l_t,$ where $\triangle\tilde{x} = \frac{\tilde{Y}}{\tan\theta} > 0.$ Suppose that the vehicle will always travel as fast as possible. Then, the travel time along line *l* is:

$$t(\lambda) = 2\left(\sqrt{\tilde{Y}}\right)\sqrt{\frac{1+\frac{1}{\lambda^2}}{2\hat{a}_1\sqrt{1+\frac{1}{\lambda^2}}-2\hat{p}_1}}, \tag{23}$$

Theorem 5. Let the assumptions in Lemma 4 hold. Further suppose that $\frac{\hat{p}_1}{\hat{a}_1} > \frac{1}{2}.$ Then, the linear path which minimizes travel time corresponds to the vehicle traveling at angle θ_* as characterized in Theorem 2, Equation (22).

Theorem 6. Let the assumptions in Lemma 4 hold. Further, suppose that $\frac{\hat{p}_1}{\hat{a}_1} \leq \frac{1}{2}$. Then, the linear path which minimizes travel time is the normal line connecting (0,0,0) to l_t. That is, $\theta_* = \frac{\pi}{2}$.

Discussion

In Theorems 2 and 3, we characterized the heading angle corresponding to the optimal linear path from a point in the engage line to the shoreline when the vehicle starts at rest. Additionally, we gave a realistic scenario when the optimal heading angle is significantly different than the angle perpendicular to the shoreline.

The characterization of the optimal heading angle in Equation (22) has an intuitive interpretation. Define the constant:

$$\zeta = \frac{\sin\alpha}{\mu - c_{rr}\cos\alpha} \tag{23}$$

Now rewrite Equation (22) as:

$$\theta_* = \tan^{-1}\left(\sqrt{\frac{1}{4\zeta^2 - 1}}\right) \tag{24}$$

Observe that for constant μ and c_{rr}, as $\alpha \to 0,\ \zeta \to 0,$ which makes Equation (24) not suitable. However, according to Theorem 2, as $\zeta \to \frac{1}{2},\ \theta_* \to \frac{\pi}{2}.$ Intuitively, this can be understood as saying that for fixed μ and c_{rr}, there exists a sufficiently small α, not necessary equal to 0, such that the fastest linear path is the perpendicular path.

On the other hand, observe that for constant μ and c_{rr}, as $\alpha \to \frac{\pi}{2},\ \zeta \to \frac{1}{\mu} > 0.$ Intuitively, this can be understood as saying that for fixed μ and c_{rr}, there exists a strictly positive lower bound to the optimal heading angle for linear paths, regardless of α. In other words, at a certain point, reducing the effect of effective tangential weight will not save time.

In “Implications/Analysis of the Force Model”, it was shown that the optimal path had the same form whether in the transition or on a hill on dry land. In other words, the effective weight has no effect on the orientation of the optimal linear path. The key to understanding when the optimal linear path will be perpendicular to the shoreline or not is the ζ term. When $\zeta > \frac{1}{2},$ the fastest linear path is not perpendicular. This happens when the incline angle is sufficiently large, and more importantly, the difference between the friction coefficient and the rolling resistance coefficient is sufficiently small. This can happen in the transition, as well as on sloped land that has a slippery surface.

Conclusions

Summary

Several accomplishments were achieved in this report. An original baseline model was proposed for the transition, which is the operating region where an amphibious vehicle's wheels or tracks are engaged with the sea-floor, at the same time as the vehicle itself is partially submerged in water. The model developed takes into account the ground propulsive force, gravity, buoyancy, sliding friction between tires/tracks and sea-floor, rolling resistance of tires/tracks and sea-floor, and engine and drivetrain characteristics, including engine torque, gear ratios, efficiency of the drive system, and the inertia of the engine and drivetrain components. The model ignores drag, waves, currents, and other surf zone forces, which are to be addressed in future work. It also assumes ideal properties about the shape of the transition.

Using the model, novel observations were made about route optimality. Consider $\zeta = \sin\alpha/(\mu - c_{rr}\cos\alpha)$, where α is the angle of inclination of the transition hill, μ is the peak sliding friction coefficient between the tires/tracks and the sea-floor, and c_{rr} is the rolling resistance coefficient between the tires/tracks and sea-floor. It was shown that when $\zeta > ½$, the fastest path for the vehicle to traverse in the transition *is not* perpendicular to the shoreline. Moreover, realistic cases were found when $\zeta > ½$. For this case, a closed-form characterization for the heading angle corresponding to fastest linear path was found: $\theta_* = \tan^{-1}(\sqrt{1/(4\zeta^2 - 1)})$, where a heading angle of 0^0 corresponds to traveling parallel to the shoreline and a heading angle of 90^0 corresponds to traveling perpendicular towards the shoreline.

Future Work

In our current model, we do not impose an upper bound for vehicle speed. In reality, in addition to the position and heading angle, the maximum acceleration is also dependent on the vehicle's speed, so Equation (20) does not fully capture the maximum acceleration. This factor should be considered in the future.

In calculating the travel time along a linear path, it was assumed that the vehicle's initial speed was zero. In the future, we plan to relax this assumption and evaluate the optimal linear path for a general starting speed. Then, even if the starting speed is zero at the engage line, as the vehicle travels up the transition, the optimal linear path from its present position to the shoreline will change. Even though, as stated earlier, maneuvering precisely in the transition would be very challenging, a piecewise linear path could still be feasible.

Besides loss of optimality, there is a potential loss of feasibility with a strictly linear path. Throughout this paper, we assumed that there is no bound on the $\tilde{x}$-axis of feasible "land entry points." If the bound were present, Theorems 5 and 9 would yield unfeasible trajectories. We plan to address this limitation in future research.

More work must be done to add realism to the model proposed in this report. In particular, wave and current forces in the transition are likely to noticeably influence the dynamics of the vehicle. Also, the transition might not be a planar hill, and more general transition geometries should be incorporated into the model. Similarly, the displaced water volume is not necessarily a linear function of the draft, so analysis incorporating specific hull forms into the model to calculate the buoyancy more precisely is needed. Finally, it is ultimately desired to integrate obstacles into the model because on a real beach, not all paths will be feasible.

Recommendations

The model and algorithms discussed in this report are ready to be tested in controlled environments. The model beach would have to be close to planar and the water would have to be calm. Before testing this model on DUKW-ling, various tests need be done on the DUKW-ling itself to characterize certain properties, such as the peak friction coefficient and rolling resistance between the wheels and sea-floor, which are pieces of information that are taken for granted in this report.

Appendices

Appendix A – Proofs

Proof of Lemma 1. Before we begin the proof, first recall that for a position dependent acceleration along a straight line *l*, denoted *a(s)*, where $s \in l$, the velocity at *s* is equal to (Pestel, 1968):

$$v(s) = \sqrt{v^2(s_0) + 2\int_{s_0}^{s} a(\tau)d\tau}, \tag{25}$$

where *v(s)* is the velocity at position *s*, and $v(s_0)$ is the velocity at some initial position s_0. The approach we use in this proof is to interpret the integral term in Equation (A1) as a line integral, and then to find convenient bijective (one-to-one and onto) parameterizations to simplify the calculations.

Indeed, since *l* is a straight line segment in the plane spanned by the $\tilde{x}$ and $\tilde{y}$ axis, we know that the following is a bijective parameterization of *l*: $\boldsymbol{r} : [0, \triangle\tilde{x}] \rightarrow l$ defined by $\mathbf{r}(\tilde{x}) = (\tilde{x}, \lambda\tilde{x})$, where $\lambda = \frac{\tilde{Y}}{\triangle\tilde{x}}$. As can be seen in Figure 15,

$$\sin\theta = \frac{\tilde{Y}}{\sqrt{\triangle\tilde{x}^2 + \tilde{Y}^2}} = \frac{\tilde{Y}}{\sqrt{\frac{\tilde{Y}^2}{\lambda^2} + \tilde{Y}^2}} = \frac{1}{\sqrt{1 + \frac{1}{\lambda^2}}} \tag{26}$$

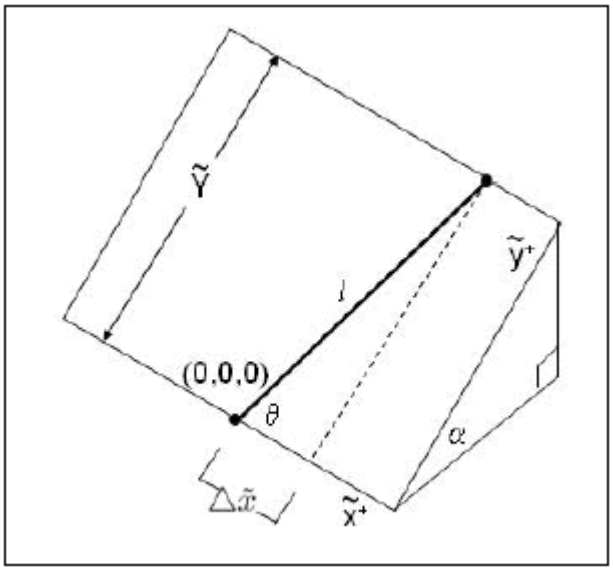

Figure 15: Arbitrary linear trajectory, (*l*), from origin to point on shoreline.

Substituting Equation (26) into Equation (20) yields a characterization of the acceleration on an arbitrary linear path with a corresponding λ:

$$a(\tilde{x},\tilde{y},\lambda) = \hat{a}_1 + \hat{a}_2\tilde{y} - \frac{\hat{p}_1 + \hat{p}_2\tilde{y}}{\sqrt{1+\frac{1}{\lambda^2}}} \tag{27}$$

For an arbitrary $(u,v,E((u,v))) \in l$, let $l_{(u,v)} \subset l$ be the straight line segment connecting (0,0,0) to (*u,v,E((u,v))*). Since, by assumption, the tractive force of the vehicle is always equal to its maximum tractive force, and the initial speed is 0, from Equation (25), we have:

$$v(u,v,\lambda) = \sqrt{2\int_{l_{(u,v)}} a(\tau)\,d\tau} \tag{28}$$

Observe that restricting **r** to the domain $[0,u] \subset [0,\Delta\tilde{x}]$ is a bijective parameterization of $l_{(u,v)}$. Note that $\frac{\mathbf{dr}}{\mathbf{d\tilde{x}}}(\tilde{x}) = (1,\lambda) \Rightarrow \left\|\frac{\mathbf{dr}}{\mathbf{d\tilde{x}}}(\tilde{x})\right\| = \sqrt{1+\lambda^2}$. By definition of line integral, it follows:

$$\int_{l_{(\tilde{x},\tilde{y})}} a(\tau)\,d\tau = \int_0^{\tilde{y}/\lambda} a(\mathbf{r}(\tilde{x}))\left\|\frac{\mathbf{dr}}{\mathbf{d\tilde{x}}}(\tilde{x})\right\| d\tilde{x}, \tag{29}$$

which, from Equation (28), implies:

$$v\left(\tilde{x},\tilde{y},\lambda\right)=\sqrt{2\sqrt{1+\lambda^2}\int_0^{\tilde{y}/\lambda}a\left(\tilde{x},\lambda\tilde{x},\lambda\right)d\tilde{x}} \tag{30}$$

Evaluating the integral using Equation (27) yields:

$$\begin{aligned}
\int_0^{\tilde{y}/\lambda}a\left(\tilde{x},\lambda\tilde{x},\lambda\right)d\tilde{x} &= \int_0^{\tilde{y}/\lambda}\left(\hat{a}_1+\hat{a}_2\lambda\tilde{x}-\frac{\hat{p}_1+\hat{p}_2\lambda\tilde{x}}{\sqrt{1+\frac{1}{\lambda^2}}}\right)d\tilde{x}\\
&= \int_0^{\tilde{y}/\lambda}\left[\left(\hat{a}_1-\frac{\hat{p}_1}{\sqrt{1+\frac{1}{\lambda^2}}}\right)+\left(\hat{a}_2\lambda-\frac{\hat{p}_2\lambda}{\sqrt{1+\frac{1}{\lambda^2}}}\right)\tilde{x}\right]d\tilde{x}\\
&= \int_0^{\tilde{y}/\lambda}\left[\left(\hat{a}_1-\frac{\hat{p}_1}{\sqrt{1+\frac{1}{\lambda^2}}}\right)+\left(\hat{a}_2\lambda-\frac{\hat{p}_2\lambda}{\sqrt{1+\frac{1}{\lambda^2}}}\right)\tilde{x}\right]d\tilde{x}\\
&= \left[\left(\hat{a}_1-\frac{\hat{p}_1}{\sqrt{1+\frac{1}{\lambda^2}}}\right)\tilde{x}+\left(\hat{a}_2\lambda-\frac{\hat{p}_2\lambda}{\sqrt{1+\frac{1}{\lambda^2}}}\right)\tilde{x}^2\right]\Big|_0^{\tilde{y}/\lambda}\\
&= \left(\hat{a}_1-\frac{\hat{p}_1}{\sqrt{1+\frac{1}{\lambda^2}}}\right)\frac{\tilde{y}}{\lambda}+\left(\hat{a}_2\lambda-\frac{\hat{p}_2\lambda}{\sqrt{1+\frac{1}{\lambda^2}}}\right)\frac{\tilde{y}^2}{\lambda^2}
\end{aligned} \tag{31}$$

So:

$$v\left(\tilde{x},\tilde{y},\lambda\right)=\sqrt{\frac{2\sqrt{1+\lambda^2}}{\lambda}\left(\left(\hat{a}_1-\frac{\hat{p}_1}{\sqrt{1+\frac{1}{\lambda^2}}}\right)\tilde{y}+\left(\hat{a}_2-\frac{\hat{p}_2}{\sqrt{1+\frac{1}{\lambda^2}}}\right)\tilde{y}^2\right)} \tag{32}$$

The critical observation is that $\frac{\hat{a}_1}{\hat{a}_2}=\frac{\hat{p}_1}{\hat{p}_2}$, which we call $k=\frac{mg}{\rho g\frac{V_H}{H}\sin\alpha}-\tilde{Y}$.
This implies:

$$\begin{aligned} v(\tilde{x},\tilde{y},\lambda) &= \left(\sqrt{2\sqrt{1+\frac{1}{\lambda^2}}\left(\hat{a}_2-\frac{\hat{p}_2}{\sqrt{1+\frac{1}{\lambda^2}}}\right)}\right)\sqrt{k\tilde{y}+\tilde{y}^2} \\ &= \left(\sqrt{2\hat{a}_2\sqrt{1+\frac{1}{\lambda^2}}-2\hat{p}_2}\right)\sqrt{\left(\tilde{y}+\frac{1}{2}k\right)^2-\frac{1}{4}k^2} \end{aligned} \tag{33}$$

Now we make another bijective parameterization of *l*, called $\boldsymbol{q}:[0,\tilde{Y}]\rightarrow l$, defined by $\mathbf{q}(\tilde{y})=\left(\frac{\tilde{y}}{\lambda},\tilde{y}\right)\Rightarrow\mathbf{q}'(\tilde{y})=\left(\frac{1}{\lambda},1\right)\Rightarrow|\mathbf{q}'(\tilde{y})|=\sqrt{1+\frac{1}{\lambda^2}}$. Again, using line integrals, we now solve for travel time:

$$\begin{aligned} t(\lambda) &= \int_l\frac{1}{v}dl=\int_0^{\tilde{Y}}\frac{d\tilde{y}}{v(\mathbf{q}(\tilde{y}),\lambda)}|\mathbf{q}'(\tilde{y})| \\ &= \sqrt{1+\frac{1}{\lambda^2}}\int_0^{\tilde{Y}}\frac{d\tilde{y}}{v\left(\frac{\tilde{y}}{\lambda},\tilde{y},\lambda\right)} \\ &= \sqrt{\frac{1+\frac{1}{\lambda^2}}{\hat{a}_2\sqrt{1+\frac{1}{\lambda^2}}-\hat{p}_2}}\int_0^{\tilde{Y}}\frac{d\tilde{y}}{\sqrt{(\tilde{y}+k)^2-k^2}}, \end{aligned} \tag{34}$$

□

Proof of Theorem 2. We differentiate the result of Lemma 1, Equation (21):

$$\begin{aligned}
\frac{dt}{d\lambda}(\lambda) &= \left(\frac{\frac{1}{2}K}{\sqrt{\frac{1+\frac{1}{\lambda^2}}{\hat{a}_2\sqrt{1+\frac{1}{\lambda^2}}-\hat{p}_2}}}\right)\left(\frac{\left(\hat{a}_2\sqrt{1+\frac{1}{\lambda^2}}-\hat{p}_2\right)\left(\frac{-2}{\lambda^3}\right)-\left(1+\frac{1}{\lambda^2}\right)\left(\frac{\frac{1}{2}\hat{a}_2}{\sqrt{1+\frac{1}{\lambda^2}}}\right)\left(\frac{-2}{\lambda^3}\right)}{\left(\hat{a}_2\sqrt{1+\frac{1}{\lambda^2}}-\hat{p}_2\right)^2}\right) \\
&= \left(\frac{1}{2}K\right)\frac{\left(\hat{a}_2\sqrt{1+\frac{1}{\lambda^2}}-\hat{p}_2\right)^{1/2}}{\sqrt{1+\frac{1}{\lambda^2}}} * \frac{2\left(\frac{\hat{p}_2-\hat{a}_2\sqrt{1+\frac{1}{\lambda^2}}}{\lambda^3}\right)+\frac{\hat{a}_2\left(1+\frac{1}{\lambda^2}\right)}{\lambda^3\sqrt{1+\frac{1}{\lambda^2}}}}{\left(\hat{a}_2\sqrt{1+\frac{1}{\lambda^2}}-\hat{p}_2\right)^2} \\
&= \left(\frac{1}{2}K\right)\frac{2\hat{p}_2-2\hat{a}_2\sqrt{1+\frac{1}{\lambda^2}}+\hat{a}_2\sqrt{1+\frac{1}{\lambda^2}}}{\lambda^3\sqrt{1+\frac{1}{\lambda^2}}\left(\hat{a}_2\sqrt{1+\frac{1}{\lambda^2}}-\hat{p}_2\right)^{3/2}} \\
&= \left(\frac{1}{2}K\right)\frac{2\hat{p}_2-\hat{a}_2\sqrt{1+\frac{1}{\lambda^2}}}{\lambda^3\sqrt{1+\frac{1}{\lambda^2}}\left(\hat{a}_2\sqrt{1+\frac{1}{\lambda^2}}-\hat{p}_2\right)^{3/2}} \qquad (35)
\end{aligned}$$

To find the critical value, denoted λ_*, we set $\frac{dt}{d\lambda}(\lambda_*)=0$, which implies:

$$2\hat{p}_2-\hat{a}_2\sqrt{1+\frac{1}{\lambda_*^2}}=0 \Rightarrow \sqrt{1+\frac{1}{\lambda_*^2}}=2\frac{\hat{p}_2}{\hat{a}_2} \Rightarrow 1+\frac{1}{\lambda_*^2}=4\left(\frac{\hat{p}_2}{\hat{a}_2}\right)^2 \Rightarrow$$

$$\frac{1}{\lambda_*^2}=4\left(\frac{\hat{p}_2}{\hat{a}_2}\right)^2-1 \quad \Rightarrow \qquad (36)$$

$$\lambda_*=\sqrt{\frac{1}{4\left(\frac{\hat{p}_2}{\hat{a}_2}\right)^2-1}} \qquad (37)$$

Suppose λ_* were a minimizer of *t*. then, there must be a corresponding $\triangle\tilde{x}_*$ such that $\lambda_*=\frac{\tilde{Y}}{\triangle\tilde{x}_*}=\tan\theta_*$, where θ_* is the heading angle corresponding to the linear path associated with λ_*, or the optimal linear path. Equation (22) then immediately follows, which is what we wished to show.

It remains to be shown that λ_* is indeed a minimizer of *t*. It suffices to show that $\lambda>\lambda_* \Rightarrow \frac{dt}{d\lambda}(\lambda)>0$ and $\lambda<\lambda_* \Rightarrow \frac{dt}{d\lambda}(\lambda)<0$. Since the denominator in Equation

(35) is strictly positive, it suffices to show that $\lambda > \lambda_* \Rightarrow 2\hat{p}_2\sqrt{1+\frac{1}{\lambda^2}} - \hat{a}_2\left(1+\frac{1}{\lambda^2}\right) > 0$ and $\lambda < \lambda_* \Rightarrow 2\hat{p}_2\sqrt{1+\frac{1}{\lambda^2}} - \hat{a}_2\left(1+\frac{1}{\lambda^2}\right) < 0.$ Indeed, suppose $\lambda < \lambda_*$. It follows:

$$\lambda^2 < \lambda_*^2 = \frac{1}{4\left(\frac{\hat{p}_2}{\hat{a}_2}\right)^2 - 1} \Rightarrow 4\left(\frac{\hat{p}_2}{\hat{a}_2}\right)^2 - 1 < \frac{1}{\lambda^2} \Rightarrow$$
$$4\left(\frac{\hat{p}_2}{\hat{a}_2}\right)^2 < \frac{1}{\lambda^2} + 1 \Rightarrow 2\left(\frac{\hat{p}_2}{\hat{a}_2}\right) < \sqrt{1+\frac{1}{\lambda^2}} \Rightarrow$$
$$2\left(\frac{\hat{p}_2}{\hat{a}_2}\right)\sqrt{1+\frac{1}{\lambda^2}} < \frac{1}{\lambda^2} + 1 \Rightarrow$$
$$2\hat{p}_2\sqrt{1+\frac{1}{\lambda^2}} - \hat{a}_2\left(1+\frac{1}{\lambda^2}\right) < 0 \qquad (38)$$

Similarly, for $\lambda > \lambda_*$:

$$\lambda^2 > \lambda_*^2 = \frac{1}{4\left(\frac{\hat{p}_2}{\hat{a}_2}\right)^2 - 1} \Rightarrow 4\left(\frac{\hat{p}_2}{\hat{a}_2}\right)^2 - 1 > \frac{1}{\lambda^2} \Rightarrow$$
$$4\left(\frac{\hat{p}_2}{\hat{a}_2}\right)^2 > \frac{1}{\lambda^2} + 1 \Rightarrow 2\left(\frac{\hat{p}_2}{\hat{a}_2}\right) > \sqrt{1+\frac{1}{\lambda^2}} \Rightarrow$$
$$2\left(\frac{\hat{p}_2}{\hat{a}_2}\right)\sqrt{1+\frac{1}{\lambda^2}} > \frac{1}{\lambda^2} + 1 \Rightarrow$$
$$2\hat{p}_2\sqrt{1+\frac{1}{\lambda^2}} - \hat{a}_2\left(1+\frac{1}{\lambda^2}\right) > 0$$

(39)

□

Proof of Theorem 3. Observe:

$$\begin{aligned}
\left(\frac{\hat{p}_2}{\hat{a}_2}\right)^2 \leq \frac{1}{4} \leq \frac{1}{4}\left(1+\frac{1}{\lambda^2}\right) &\Rightarrow \\
4\left(\frac{\hat{p}_2}{\hat{a}_2}\right)^2 \leq 1+\frac{1}{\lambda^2} &\Rightarrow \\
4\hat{p}_2^2 \leq \hat{a}_2^2\left(1+\frac{1}{\lambda^2}\right) &\Rightarrow \\
4\hat{p}_2^2\left(1+\frac{1}{\lambda^2}\right) \leq \hat{a}_2^2\left(1+\frac{1}{\lambda^2}\right)^2 &\Rightarrow \\
2\hat{p}_2\sqrt{1+\frac{1}{\lambda^2}} \leq \hat{a}_2\left(1+\frac{1}{\lambda^2}\right) &\Rightarrow \\
2\hat{p}_2\sqrt{1+\frac{1}{\lambda^2}} - \hat{a}_2\left(1+\frac{1}{\lambda^2}\right) \leq 0. &\qquad (40)
\end{aligned}$$

As can be seen in Equation (35), the denominator of $\frac{dt}{d\lambda}(\lambda)$ is strictly positive, so Equation (40) implies that $\frac{dt}{d\lambda}(\lambda)$ is nonincreasing, which means that as $\lambda \to \infty$, *t*(λ) gets smaller or stays the same, which means the line with slope ∞, the perpendicular line, minimizes travel time.

□

Proof of Lemma 4. Everything in the proof for Lemma 1 holds up through Equation (32). Now substitute $\hat{a}_2 = \hat{p}_2 = 0$ to get:

$$\begin{aligned}
v(\tilde{x},\tilde{y},\lambda) &= \sqrt{\frac{2\sqrt{1+\lambda^2}}{\lambda}\left(\left(\hat{a}_1 - \frac{\hat{p}_1}{\sqrt{1+\frac{1}{\lambda^2}}}\right)\tilde{y}\right)} \\
v(\tilde{x},\tilde{y},\lambda) &= \sqrt{\tilde{y}}\sqrt{2\hat{a}_1\sqrt{1+\frac{1}{\lambda^2}} - 2\hat{p}_1} \qquad (41)
\end{aligned}$$

Applying a process similar to Equation (34) yields:

$$t(\lambda) = \left(\sqrt{\frac{1+\frac{1}{\lambda^2}}{2\hat{a}_1\sqrt{1+\frac{1}{\lambda^2}} - 2\hat{p}_1}}\right)\int_0^{\tilde{Y}} \frac{1}{\tilde{y}}d\tilde{y}, \qquad (42)$$

which implies Equation (23).

□

Proof of Theorem 5. Differentiating the result of Lemma 4, Equation (23), yields:

$$\begin{aligned}
\frac{dt}{d\lambda}(\lambda) &= \frac{\sqrt{\tilde{Y}}}{\sqrt{\frac{1+\frac{1}{\lambda^2}}{2\hat{a}_1\sqrt{1+\frac{1}{\lambda^2}}-2\hat{p}_1}}} * \frac{\left(2\hat{a}_1\sqrt{1+\frac{1}{\lambda^2}}-2\hat{p}_1\right)\frac{-2}{\lambda^3}-\left(1+\frac{1}{\lambda^2}\right)\left(\frac{\hat{a}_1}{\sqrt{1+\frac{1}{\lambda^2}}}\right)\left(\frac{-2}{\lambda^3}\right)}{\left(2\hat{a}_1\sqrt{1+\frac{1}{\lambda^2}}-2\hat{p}_1\right)^2} \\
\frac{dt}{d\lambda}(\lambda) &= \frac{-2\sqrt{\tilde{Y}}\left(2\hat{a}_1\sqrt{1+\frac{1}{\lambda^2}}-2\hat{p}_1-\hat{a}_1\sqrt{1+\frac{1}{\lambda^2}}\right)}{\lambda^3\sqrt{1+\frac{1}{\lambda^2}}\left(2\hat{a}_1\sqrt{1+\frac{1}{\lambda^2}}-2\hat{p}_1\right)^{3/2}} \\
\frac{dt}{d\lambda}(\lambda) &= \frac{\sqrt{\tilde{Y}}\left(2\hat{p}_1-\hat{a}_1\sqrt{1+\frac{1}{\lambda^2}}\right)}{\lambda^3\sqrt{1+\frac{1}{\lambda^2}}\left(2\hat{a}_1\sqrt{1+\frac{1}{\lambda^2}}-2\hat{p}_1\right)^{3/2}} \qquad (43)
\end{aligned}$$

To find the critical value, denoted λ_*, we set $\frac{dt}{d\lambda}(\lambda_*)=0$, which implies:

$$2\hat{p}_1-\hat{a}_1\sqrt{1+\frac{1}{\lambda_*^2}}=0 \Rightarrow \sqrt{1+\frac{1}{\lambda_*^2}}=2\frac{\hat{p}_1}{\hat{a}_1} \Rightarrow 1+\frac{1}{\lambda_*^2}=4\left(\frac{\hat{p}_1}{\hat{a}_1}\right)^2 \Rightarrow$$

$$\frac{1}{\lambda_*^2}=4\left(\frac{\hat{p}_1}{\hat{a}_1}\right)^2-1 \quad \Rightarrow \qquad (44)$$

$$\lambda_*=\sqrt{\frac{1}{4\left(\frac{\hat{p}_1}{\hat{a}_1}\right)^2-1}} \qquad (45)$$

Suppose λ_* were a minimizer of *t*. then, there must be a corresponding $\triangle\tilde{x}_*$ such that $\lambda_*=\frac{\tilde{Y}}{\triangle\tilde{x}_*}=\tan\theta_*$, where θ_* is the heading angle corresponding to the linear path associated with λ_*, or the optimal linear path. Equation (22) then immediately follows, which is what we wished to show.

It remains to be shown that λ_* is indeed a minimizer of *t*. It suffices to show that $\lambda>\lambda_* \Rightarrow \frac{dt}{d\lambda}(\lambda)>0$ and $\lambda<\lambda_* \Rightarrow \frac{dt}{d\lambda}(\lambda)<0$. Since the denominator in Equation (43) is strictly positive, it suffices to show that $\lambda>\lambda_* \Rightarrow 2\hat{p}_2\sqrt{1+\frac{1}{\lambda^2}}-\hat{a}_2\left(1+\frac{1}{\lambda^2}\right)>0$ and $\lambda<\lambda_* \Rightarrow 2\hat{p}_2\sqrt{1+\frac{1}{\lambda^2}}-\hat{a}_2\left(1+\frac{1}{\lambda^2}\right)<0.$ Indeed, suppose $\lambda<\lambda_*$. It follows:

$$\lambda^2 < \lambda_*^2 = \frac{1}{4\left(\frac{\hat{p}_1}{\hat{a}_1}\right)^2 - 1} \Rightarrow 4\left(\frac{\hat{p}_1}{\hat{a}_1}\right)^2 - 1 < \frac{1}{\lambda^2} \Rightarrow$$

$$4\left(\frac{\hat{p}_1}{\hat{a}_1}\right)^2 < \frac{1}{\lambda^2} + 1 \Rightarrow 2\left(\frac{\hat{p}_1}{\hat{a}_1}\right) < \sqrt{1 + \frac{1}{\lambda^2}} \Rightarrow$$

$$2\left(\frac{\hat{p}_1}{\hat{a}_1}\right)\sqrt{1 + \frac{1}{\lambda^2}} < \frac{1}{\lambda^2} + 1 \Rightarrow$$

$$2\hat{p}_1\sqrt{1 + \frac{1}{\lambda^2}} - \hat{a}_1\left(1 + \frac{1}{\lambda^2}\right) < 0 \qquad (46)$$

Similarly, for $\lambda > \lambda_*$:

$$\lambda^2 > \lambda_*^2 = \frac{1}{4\left(\frac{\hat{p}_1}{\hat{a}_1}\right)^2 - 1} \Rightarrow 4\left(\frac{\hat{p}_1}{\hat{a}_1}\right)^2 - 1 > \frac{1}{\lambda^2} \Rightarrow$$

$$4\left(\frac{\hat{p}_1}{\hat{a}_1}\right)^2 > \frac{1}{\lambda^2} + 1 \Rightarrow 2\left(\frac{\hat{p}_1}{\hat{a}_1}\right) > \sqrt{1 + \frac{1}{\lambda^2}} \Rightarrow$$

$$2\left(\frac{\hat{p}_1}{\hat{a}_1}\right)\sqrt{1 + \frac{1}{\lambda^2}} > \frac{1}{\lambda^2} + 1 \Rightarrow$$

$$2\hat{p}_1\sqrt{1 + \frac{1}{\lambda^2}} - \hat{a}_1\left(1 + \frac{1}{\lambda^2}\right) > 0$$

(47)

□

Proof of Theorem 6. Using a similar procedure as the proof in Theorem 3, one can establish Theorem 6.

□

Appendix B – Works Cited

Florida Atlantic University (FAU). Control of Unmanned Amphibious Cargo Carrying System Final Design Report. *FAU Senior Design Report*, 2010.

T. D. Gillespie. *Fundamentals of Vehicle Dynamics*. Society of Automotive Engineers, Inc.; USA, 1992.

F. Gonzalez, et. al. DUKW 21 – Amphibious cargo transfer from ship to shore. *Center for Innovation in Ship Design, Naval Surface Warfare Center, Carderock Division technical report*.

E. R. Jones, R. L. Childers. *Contemporary College Physics*. McGraw-Hill Inc.; USA, 2000.

E. C. Pestel. *Dynamics*. McGraw-Hill Inc.; USA, 1968.

N.C. Rowe, R.S. Ross. Optimal grid-free path planning across arbitrarily contoured terrain with anisotropic friction and gravity effects. *IEEE Transactions on Robotics and Automation*. 6(5) 540-553, 1990.

Z. Sun, J. Reif. On finding energy-minimizing paths on terrains. *IEEE Transactions on Robotics and Automation*, 21(1):102--114, 2005.